

Multiphoton Imaging and Quantitative Analysis of Collagen Production by Chondrogenic Human Mesenchymal Stem Cells Cultured in Chitosan Scaffold

Wei-Liang Chen, Ph.D.,^{1,*} Chi-Hsiu Huang, M.S.,^{1,*} Ling-Ling Chiou, B.Sc.,²
Te-Hsuen Chen, M.S.,³ Yi-You Huang, Ph.D.,³ Ching-Chuan Jiang, M.D.,⁴
Hsuan-Shu Lee, M.D.,^{2,5} and Chen-Yuan Dong, Ph.D.^{1,6,7}

We used the combined imaging modality of multiphoton autofluorescence and second-harmonic generation microscopy to investigate the chondrogenic process of human mesenchymal stem cells cultured in chitosan scaffold. Isolated human mesenchymal stem cells seeded onto chitosan scaffold were induced to undergo chondrogenesis by addition of the transforming growth factor- β 3. After continuous culturing, the engineered tissues at the same scaffold location were imaged at different time points for up to 49 days. Using the acquired images of the chondrogenic process, we quantify tissue morphogenesis by monitoring the changes in multiphoton autofluorescence and second-harmonic generation signals from the engineered tissues. We found that the extracellular matrix generation can be modeled by an exponential function during the initial growth stage and that saturation occurs between days 11 and 14. Further, the growth rate of the extracellular matrix was found to increase toward the surface of the chitosan scaffold. Our work demonstrates the use of multiphoton microscopy for performing long-term monitoring and quantification of the tissue engineering process.

Introduction

THE IDEA OF USING STEM CELLS to cultivate usable tissues for organ repair holds tremendous promise.¹⁻³ Human mesenchymal stem cells (hMSCs) derived from bone marrow offer such a possibility. At this point, the transformation of stem cells into the appropriate cell type and the physiological processes governing the transformed tissues is not completely understood.⁴ However, most optical examinations of engineered tissues are accomplished by traditional histological examination with a number of drawbacks. Histological images are temporal snapshots of fixed tissues, and the details of subsequent physiological mechanism cannot be investigated. In addition, there is a need of a minimally invasive imaging modality that can monitor the morphological and functional states of the engineered tissues. Quantitative analysis and modeling of such image monitoring can act as a

quality control check of the engineered tissues and are necessary for evaluating the appropriateness of the engineered tissues for transplantation. Clearly, a qualitative and quantitative diagnostic tool for evaluating the engineered tissues before implantation will be of tremendous value to stem cell research and tissue engineering. Although confocal imaging is the dominant technique for obtaining microscopic structural information in stem cell research,⁵⁻⁸ this approach can lead to out-of-focus photodamage, and the use of a confocal aperture can decrease signal strength due to sample scattering.

One promising technique that may address the need of stem cell biology and tissue engineering for minimally invasive three-dimensional cellular imaging is multiphoton microscopy. Pioneers of this technique used either multiphoton fluorescence excitation or the harmonic generation process to achieve imaging of biological tissues.⁹⁻¹² In the

¹Department of Physics, National Taiwan University, Taipei, Taiwan.

²Department of Internal Medicine, National Taiwan University Hospital and National Taiwan University College of Medicine, Taipei, Taiwan.

³Institute of Biomedical Engineering, National Taiwan University, Taipei, Taiwan.

⁴Department of Orthopedics, National Taiwan University Hospital, Taipei, Taiwan.

⁵Institute of Biotechnology, ⁶Center for Quantum Science and Engineering, and ⁷Biomedical Molecular Imaging Core, Division of Genomics, NTU Research Center for Medical Excellence, National Taiwan University, Taipei, Taiwan.

*These two authors contributed equally to this work.

fluorescence mode, fluorescent molecules typically excited by ultraviolet or visible photons are induced to reach the excited states by the absorption of two or more near-infrared photons. In the harmonic generation mode, the nonlinear polarization of the tissue of interest is explored for imaging purposes. In biological tissues with noncentrosymmetric molecular structures, $P_i^{(2)}$, the second-order polarization effect induced by the external electric field, E , is given by

$$P_i^{(2)} = \chi_{ijk} E_j E_k, \quad (1)$$

wherein χ_{ijk} is the second-order susceptibility tensor. The second-harmonic generation (SHG) effect can be used to effectively image tissues such as collagen and muscle fibers.¹²⁻¹⁴ Among the features of multiphoton microscopy are point-like excitation and enhanced depth penetration. For tissue imaging, the confocal-like imaging quality and axial-depth discrimination feature resulting from point-like excitation within the specimen allow confocal-like image quality to be achieved without the use of confocal aperture, and the greatly reduced photodamage resulting from the point-like excitation limits specimen photodamage to the focal volume. The latter feature is especially significant for tissue engineering and stem cell biology study, if one were to achieve long-term, noninvasive characterization of the engineered tissues. Specifically, an advantage of this methodology is prolonged specimen longevity.¹⁵ In this work, we performed multiphoton autofluorescence (MAF) and SHG microscopy on engineered tissues synthesized from hMSCs cultured onto chitosan scaffolds. In a previous study, the use of PGA as a scaffold for collagen production led to scaffold structural change,^{16,17} which prevented the use of quantitative analysis over the same region, and the application of a physical model for describing extracellular matrix (ECM) growth. In this work, we use chitosan for improved scaffold structural integrity, which allows us to return to the same location for

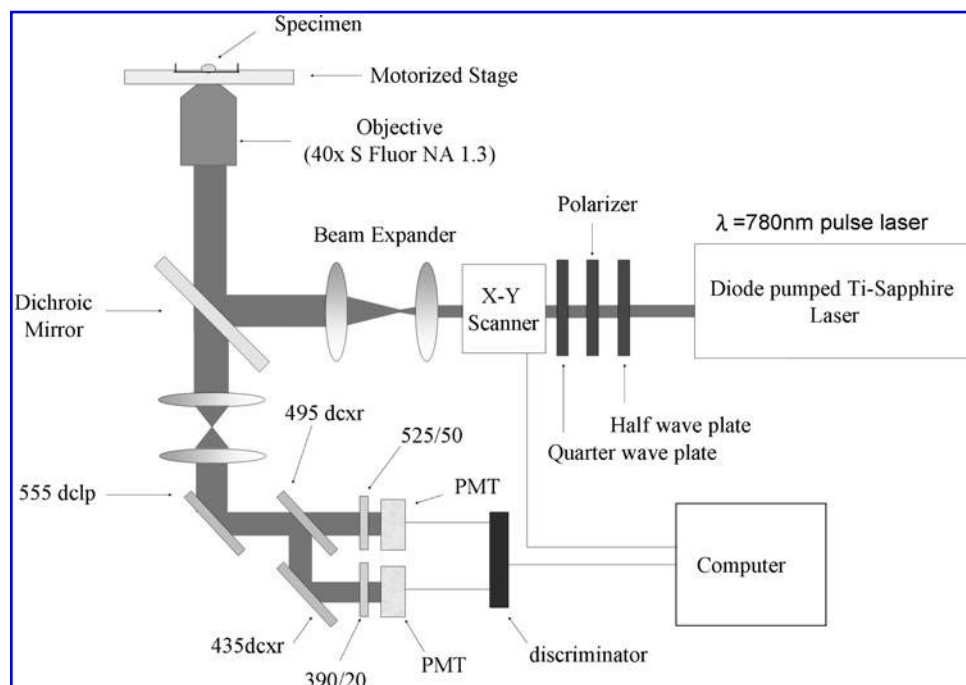
long-term imaging. By imaging and analyzing the same location in the scaffold over an extended period, we show that the growth and development of the engineered tissue constructs from hMSCs can be followed with minimal invasion.

Materials and Methods

Multiphoton microscopy

A schematic diagram of the MAF and SHG microscope used in this study is shown in Figure 1. Our system is composed of a custom-built laser scanning microscope imaging system constructed from an inverted microscope (TE2000U; Nikon, Tokyo, Japan). For MAF and SHG imaging, a diode-pumped, solid-state (Millennia X; Spectra Physics, Mountain View, CA) pumped titanium-sapphire laser (Tsunami; Spectra Physics) producing 80-MHz femto-second laser pulses was used as the excitation source. In this study, the laser was tuned to 780 nm for both MAF and SHG production. The computer-controlled galvanometer scanning system (Model 6220; Cambridge Technology, Cambridge, MA) steers the laser source in two dimensions. The scanned laser beam is expanded and then reflected by the primary dichroic mirror (700DCSPXRUV-3p; Chroma Technology, Rockingham, VT) into the back aperture of an oil-immersion objective (S Fluor 40 \times , NA 1.3; Nikon). The epi-illuminated MAF and backward SHG signals are then collected by the same objective and passed through the primary dichroic onto the photodetectors. Before reaching the detectors, spectrally resolved autofluorescence and the SHG signals are separated by the combination of dichroic mirrors (555dclp, 495dcxr, 435dcxr; Chroma Technology) and filters (HQ525/50, HQ390/20; Chroma Technology). The detection bandwidths for autofluorescence and the SHG signals were 500–550 nm and 380–400 nm, respectively. All signals were detected by single-photon-counting photomultiplier tubes (R7400P; Hamamatsu, Hamamatsu City, Japan). For large-area scanning

FIG. 1. Diagram of the multiphoton autofluorescence (MAF) and second-harmonic generation (SHG) microscope used in this experiment.



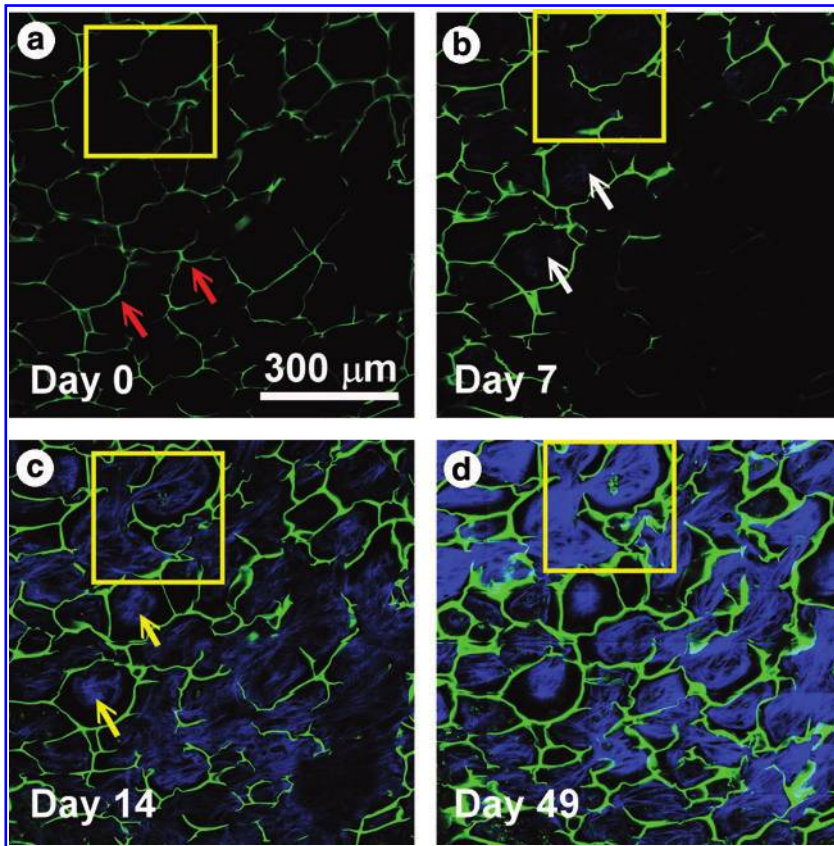


FIG. 2. Large-area MAF and SHG images of engineered tissues from human mesenchymal stem cells cultured in chitosan scaffold. Representative images shown were acquired at the depth of 15 μm on (a) day 0, (b) day 7, (c) day 14, and (d) day 49. The green represents MAF, and the blue represents SHG. Red arrows in (a) show that the scaffold boundaries can be delineated by MAF. At day 7, traces of second-harmonic generating fibers are visible (white arrows, b). By day 14, globular masses of SHG fibers are visible (yellow arrows, c). Color images available online at www.liebertonline.com/ten.

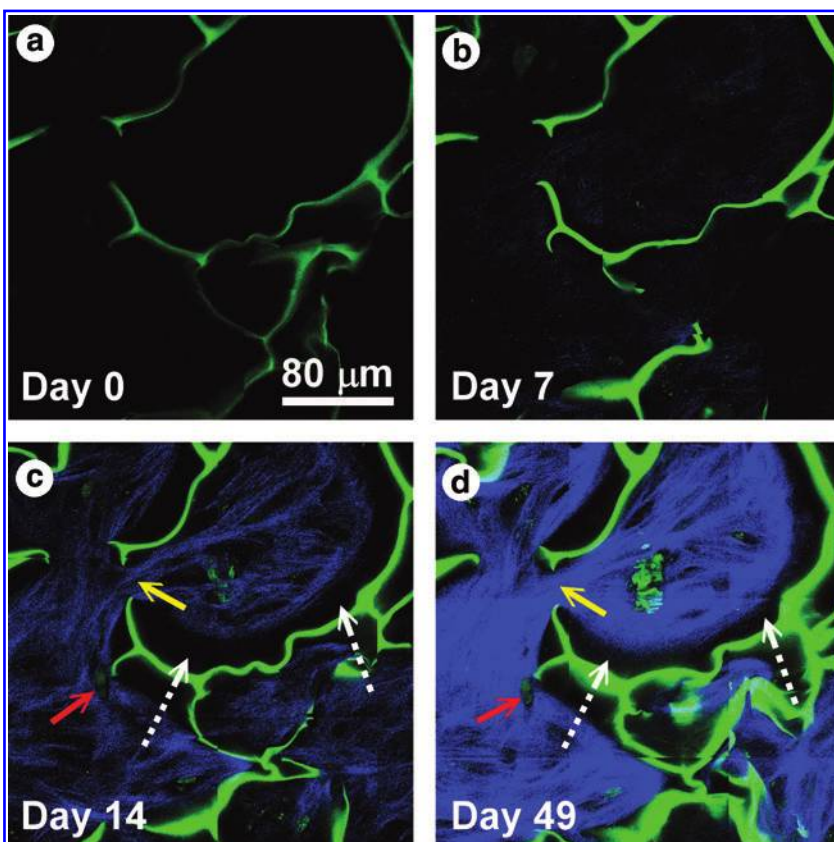


FIG. 3. Magnified multiphoton image of selected regions of interest at (a) day 0, (b) day 7, (c) day 14, and (d) day 49 of Figure 2 (boxed regions). The green represents MAF, and the blue represents SHG. The lack of contact between the induced collagen fibers and the chitosan scaffold is shown by the white dashed arrows, and the linkages formed by the collagen from adjacent chitosan domains are shown by the yellow arrows. The red arrows show the lacunae-like structures that have been formed within collagen clusters, with autofluorescent cells inside. Color images available online at www.liebertonline.com/ten.

in two and three dimensions, a computer-controlled, motorized sample translation stage (H101; Prior Scientific Instruments, Cambridge, United Kingdom) was used in conjunction with the scanning software. In addition, the imaging microscope was surrounded by a thermally insulating enclosure, with the temperature of the imaging area kept constant at the physiological temperature of 37°C.

hMSC preparation

The procurement and preparation of the hMSCs used in this study have been previously described.¹⁶ Bone marrow samples were procured with written informed consent from patients who had undergone total hip surgery. The hMSCs obtained from the bone marrow were suspended in Dulbecco's modified Eagle's medium-low glucose (Gibco, Grand Island, NY) supplemented with 10% fetal bovine serum, 10 U/mL penicillin G, and 10 µg/mL streptomycin. Drops of the cell-medium suspension were then added to both sides of a 1 mm thick, 3 mm×3 mm piece of chitosan scaffold.

Chitosan scaffold preparation

The chitosan/acetic acid solution (2% w/v) was poured into a 3.5-cm tissue culture dish and frozen at -20°C for 24 h. The chitosan scaffold was then washed with 1 M NaOH/methanol aqueous solution for 10 min followed by another 10 min wash with water. Finally, methanol solution (50% w/v) was used to wash the scaffold until the pH became 7. The scaffold was stirred with methanol solution (99% w/v) for 20 min and lyophilized in a freeze-dryer (VIRTIS, Warminster, PA) to remove the residual methanol. All chemical reagents had been purchased from Sigma (St. Louis, MO).

Sample preparation

The chitosan scaffold and the MSCs were cultured in a humidified 5% CO₂ incubator at 37°C for 1 day before the scaffold was glued onto the cover glass of a glass bottom dish with a tissue adhesive (Histoacryl®; B. Braun, Melsungen, Germany). Gluing the scaffold onto the cover glass allowed us to image the same area over the course of the experiment. During the period of experiment, the scaffold and the MSCs were cultured in a medium that contained transforming growth factor-β3 (TGF-β3; R&D Systems, Minneapolis, MN) to induce the differentiation of MSCs into chondrocytes. The medium was changed every 3 days, and the samples were imaged before the addition of medium with TGF-β3 (day 0) and on days 7, 11, 14, 21, 28, and 49 after introduction of the TGF-β3 containing culturing medium. In this study, three separately prepared MSC-chitosan specimens were imaged and analyzed.

Results and Discussion

A set of representative, large-area MAF and SHG images of the stem cell/chitosan system is shown in Figure 2. These images were acquired at the approximate depth of 15 µm, and they represent multiphoton images acquired of the same synthesized tissues at days 0, 7, 14, and 49, respectively. In Figure 2 and subsequent figures, the green pseudo color represents the specimen autofluorescence signal from 500 to 550 nm, and the blue pseudo color represents the SHG signal

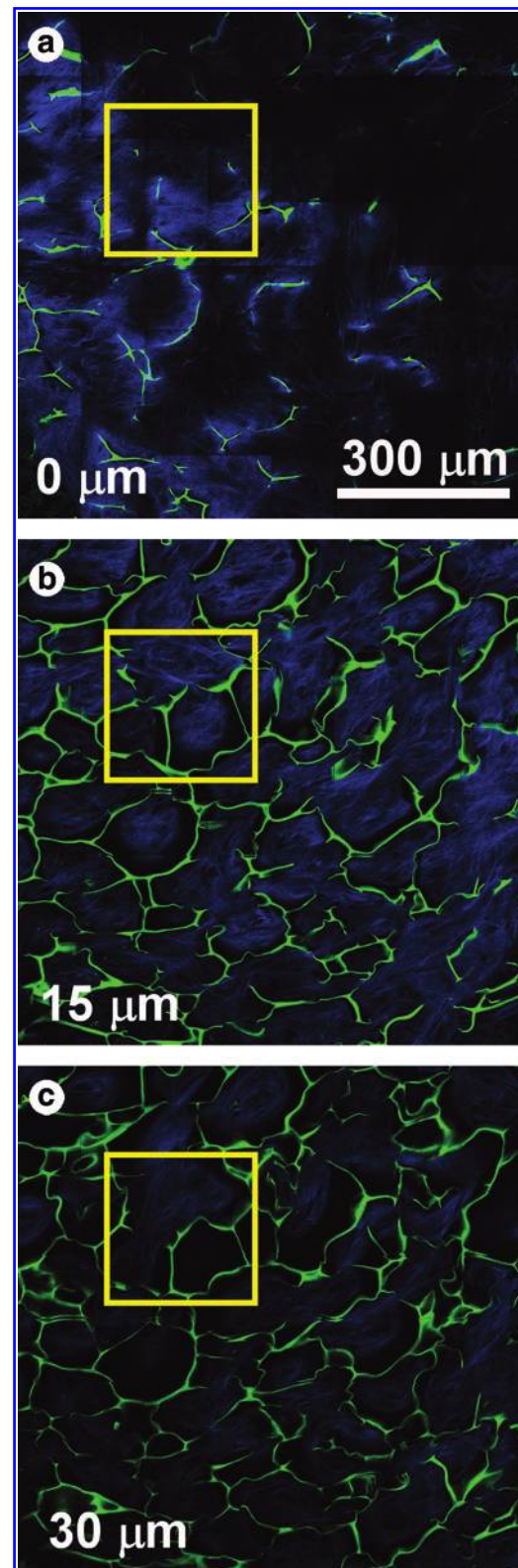


FIG. 4. Large-area MAF and SHG images of engineered tissues from human mesenchymal stem cells cultured in chitosan scaffold on day 21 and at the depths of (a) 0 µm, (b) 15 µm, and (c) 30 µm (green, MAF; blue, SHG). Color images available online at www.liebertonline.com/ten.

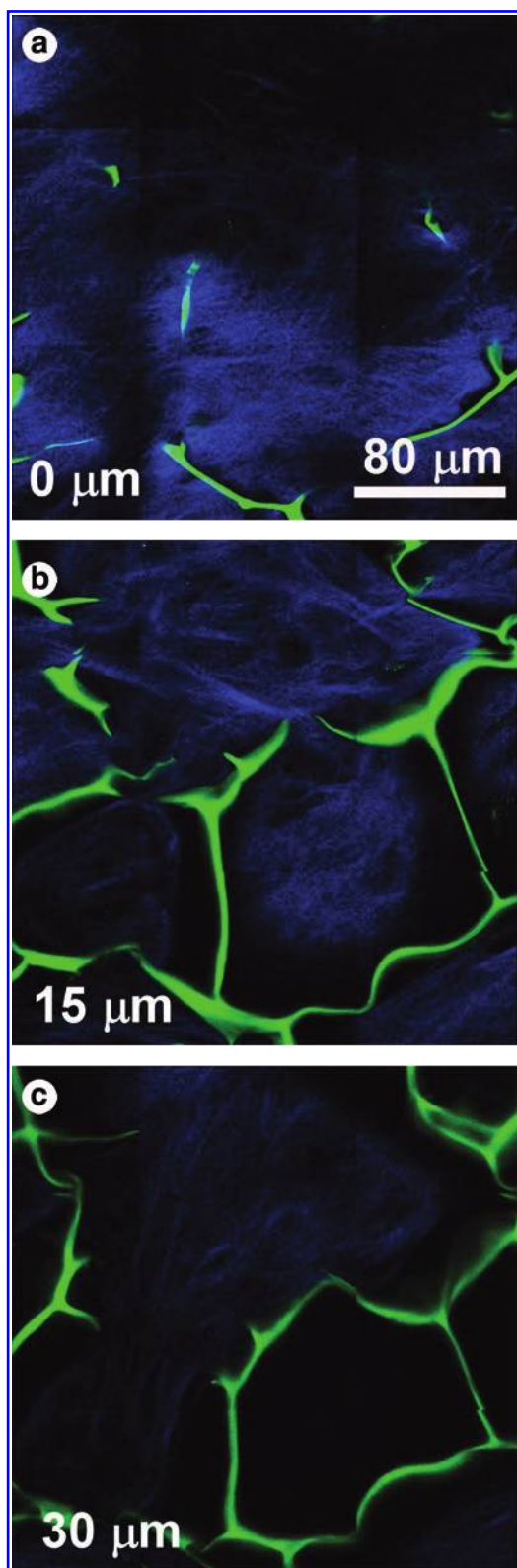


FIG. 5. Magnified MAF and SHG images of selected regions of interest on day 21 and at the depths of (a) $0\ \mu\text{m}$, (b) $15\ \mu\text{m}$, and (c) $30\ \mu\text{m}$ of Figure 4 (boxed regions) (green, MAF; blue, SHG). Color images available online at www.liebertonline.com/ten.

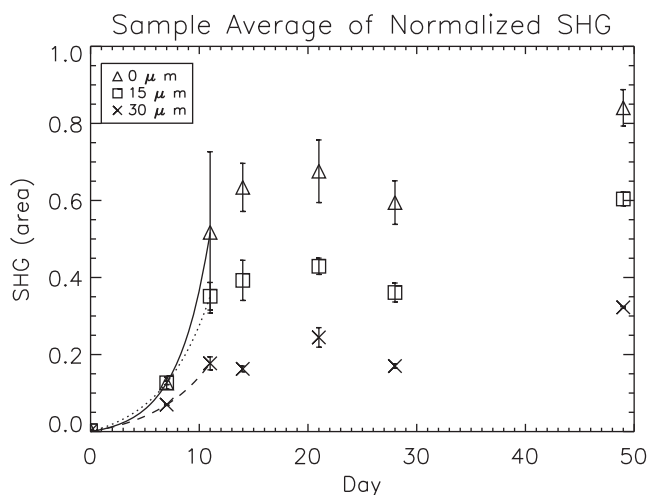


FIG. 6. Plots of the sample average of the normalized SHG as a function of induction time for the three imaging depths show saturation occurs between days 11 and 14 at all observed depth. The curves show the result of model fitting with an exponential function. The solid, short-dash, and long-dash curves show respectively the results of model fitting with an exponential function for the depth of 0, 15, and 30 microns.

centered at 390 nm. As the images demonstrate, the large-area multiphoton image shows that the chitosan scaffold is strongly autofluorescent and that the scaffold boundaries can be easily delineated (red arrows). However, without the addition of the chondrogenic induction factor TGF- β 3, one would not expect chondrogenesis to begin, as no SHG generating collagen fibers were observed on day 0. On day 7, however, traces of second-harmonic generating fibers (white arrows) became visible. We found that under the constant induction condition, the production of ECM is highly non-linear and progresses rapidly after day 7. This observation is substantiated by the day 14 image, wherein globular masses of SHG fibers can be located within the individual chitosan compartments (yellow arrows). Therefore, the geometrical

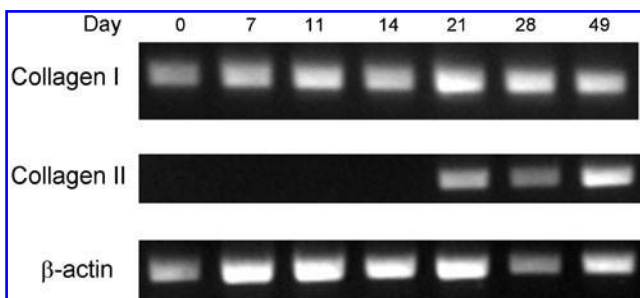
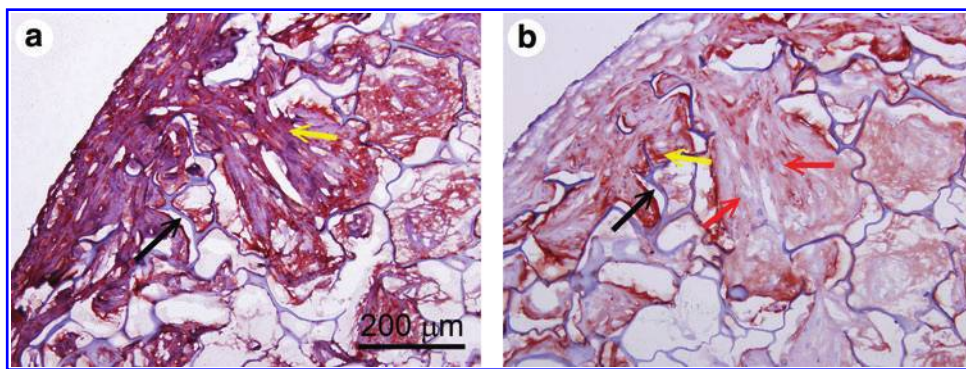


FIG. 7. RT-polymerase chain reaction (PCR) analysis of the expression of mRNA for type I and type II collagen. Reverse transcriptase-polymerase chain reaction (RT-PCR) analysis showed that the expression of type II collagen was not detected before day 21 after chondrogenic induction. Loading of PCR products of β -actin served as an internal control.

FIG. 8. Histological images of (a) type I and (b) type II immunostaining of adjacent sections of the sample used for multiphoton imaging. The location of chitosan (black arrows) and the produced collagen matrix (yellow arrows) are consistent with the multiphoton images (Figs. 2–4). The red arrows in (b) show cells inside lacunae-like structures within the collagen II matrix. Color images available online at www.liebertonline.com/ten.



constraints imposed by the scaffold materials have a substantial influence on the outcome of the morphology of cultured ECM. Qualitatively, we found that the ECM production process begins to saturate at approximately day 14, and the images at day 49 show a saturation of ECM production. Although large-area imaging provides us with a global view of induced tissues, high-resolution structural information can be visualized by magnified images. The images of the respective selected regions of interest from the results of days 0, 7, 14, and 49 in Figure 2 (boxed regions) are shown in Figure 3a–d. The enlarged images correspond to the same area in the chitosan scaffold and show several significant features of the MSC–chitosan system. First, let us notice the lack of contact between the induced collagen fibers and the chitosan scaffold with gaps between these two structures (white dashed arrows in Fig. 3c, d). As a result, the synthesized collagen fibers form clusters that are confined within individual chitosan domains. In fact, it was observed that collagen clusters between adjacent chitosan domains prefer to form mutual linkages rather than costructures with the chitosan scaffold (yellow arrows in Fig. 3c, d). In addition, individual cultured MSCs and their clusters within the collagen clusters are visible under MAF imaging. Specifically, by day 14, lacunae-like structures with autofluorescent chondrocytes found in natural cartilage begin to appear within collagen clusters (red arrows).¹⁸

To further characterize features of the MSC–chitosan system, representative, large-area MAF and SHG images of the results of day 21 acquired at the imaging depths of 0, 15, and 30 μm are shown in Figure 4. Several prominent features stand out. First, there is depth-dependence of collagen production. At the surface (0 μm), collagen production is evident with extension to regions outside the chitosan scaffold. Among the three imaging depths, observable collagen density is the highest at 0 μm and decreases with increasing depths into the chitosan scaffold. This observation is consistent with previous findings using immunohistochemical methods and is likely due to the difficulty for the cell and the collagen produced to penetrate the chitosan scaffold structure.¹⁹ Although these observations over the MSC–chitosan scaffold are global, magnified images in Figure 5 [(a) 0 μm , (b) 15 μm , and (c) 30 μm] show these features more clearly. Further, collagen cluster formation and confinement within the chitosan scaffold are found throughout the MSC–chitosan matrix.

In addition to qualitative imaging, we also attempted to quantify our observation of the collagen production process. In this effort, we determined the area of SHG at the three imaging depths (0, 15, and 30 μm) as a function of induction time (days 0, 7, 11, 14, 21, 28, and 49). Quantification of ECM production by using SHG area instead of SHG intensity avoids the effects of spherical aberration on SHG signal production. By measuring the number of pixels with SHG intensity above the background threshold value, we effectively quantify the volume inside the chitosan scaffold that has been filled with collagen ECM. The resulting SHG as a function of time at the three depths are plotted in Figure 6. The SHG for each sample are normalized with respect to the largest value for that sample over the course of the experiment, and the error bars are calculated from the standard deviation of the normalized SHG value over three samples. This quantitative analysis reveals that collagen production is nonlinear and is concentrated at the MSC–chitosan surface. Further, the saturation for collagen production occurs between days 11 and 14. By fitting the growth stage (from day 0 to 11) with an exponential function $\text{SHG} = a \cdot (e^{b \cdot t} - 1)$, wherein a is a constant, b is the growth rate, and t is time in days, we find the growth rate, b , for the depths of 0, 15, and 30 μm to be 0.33 ± 0.12 , 0.22 ± 0.03 , and 0.19 ± 0.03 , respectively. The fitted curves are shown in Figure 6 with solid, short-dash, and long-dash curves for the depths of 0, 15, and 30 μm , respectively. These results show that although the growth rate of ECM increases toward the surface of the chitosan scaffold, the saturation point is reached in about the same time for each observed depth.

Using the same reverse transcriptase-polymerase chain reaction (RT-PCR) analysis, as previously described,¹⁶ reveals that the cells found in the scaffold started to express type II collagen at day 21 (Fig. 7), whereas the multiphoton imaging shows collagen fibril production as early as day 7. Figure 8a and b show, respectively, type I and type II immunostaining of near adjacent frozen section of a sample that was used for multiphoton imaging. This sample was frozen right after the final multiphoton image acquisition (day 49). Both collagen I and II were immunostained with Mayer's hematoxylin (Sigma Aldrich, St. Louis, MO), as previously described.¹⁶ The images show that similar scaffold features can be identified in the two histological sections. Comparison of the histological images with the multiphoton images (Figs. 2–4) indicates that the location of the collagen produced (yellow arrows in Fig. 8) rel-

ative to the chitosan scaffold (black arrows in Fig. 8) is consistent with the multiphoton images. As in multiphoton images, cells inside lacunae-like spaces of the collagen II matrix are also observed (red arrows in Fig. 8b). Further, both type I and type II collagen contribute to the observed SHG signal. Although SHG imaging alone cannot separate the two types of collagen, future developments using polarization dependence of SHG may allow such distinction.²⁰

Conclusion

We demonstrated the application of MAF and SHG imaging of the TGF- β 3 induced chondrogenesis of hMSCs seeded on chitosan scaffold and found that, without extrinsic labeling, MAF allows the identification of the chitosan scaffold and imbedded MSCs, whereas the SHG signal allows the morphological characterization of the synthesized collagen. Quantitative determination of SHG further demonstrates that the saturation point is reached between days 11 and 14, and collagen production occurs more rapidly closer to the scaffold surface than the interior. The decreasing quantity of collagen produced at increasing imaging depth is likely due to the difficulty for the cells to penetrate the structure of the chitosan scaffold. This is consistent with our observation that the collagen production is confined to within individual chitosan scaffold domains and that the collagen produced internal to the scaffold have a tendency to form individual clusters with minimal interaction with the chitosan scaffold.

Our results show that qualitative and quantitative multiphoton analysis is an effective technique for monitoring synthetic tissues. Both scaffold-tissue interaction and the status of synthesized collagen matrix can be provided without invasive histological procedures. These advantages make multiphoton microscopy a potential widespread technique for noninvasive microscopic examination of the quality of engineered tissues for tissue engineering applications.

Acknowledgment

This work was supported by the National Science Council in Taiwan and was completed in the Optical Molecular Imaging Core Facility (A5) of Taiwan's National Research Program for Genomic Medicine.

Disclosure Statement

No competing financial interests exist.

References

1. Wakitani, S., Goto, T., Pineda, S.J., Young, R.G., Mansour, J.M., Caplan, A.I., and Goldberg, V.M. Mesenchymal cell-based repair of large, full-thickness defects of articular cartilage. *J Bone Joint Surg Am* **76A**, 579, 1994.
2. Alison, M.R., Poulson, R., Jeffery, R., Dhillon, A.P., Quaglia, A., Jacob, J., Novelli, M., Prentice, G., Williamson, J., and Wright, N.A. Cell differentiation—hepatocytes from non-hepatic adult stem cells. *Nature* **406**, 257, 2000.
3. Hunziker, E.B. Articular cartilage repair: basic science and clinical progress. A review of the current status and prospects. *Osteoarthritis Cartilage* **10**, 432, 2002.
4. Leo, A.J., and Grande, D.A. Mesenchymal stem cells in tissue engineering. *Cells Tissues Organs* **183**, 112, 2006.
5. Hofmann, S., Hagenmuller, H., Koch, A.M., Muller, R., Vunjak-Novakovic, G., Kaplan, D.L., Merkle, H.P., and Meinel, L. Control of *in vitro* tissue-engineered bone-like structures using human mesenchymal stem cells and porous silk scaffolds. *Biomaterials* **28**, 1152, 2007.
6. Arbab, A.S., Frenkel, V., Pandit, S.D., Anderson, S.A., Yocum, G.T., Bur, M., Khuu, H.M., Read, E.J., and Frank, J.A. Magnetic resonance imaging and confocal microscopy studies of magnetically labeled endothelial progenitor cells trafficking to sites of tumor angiogenesis. *Stem Cells* **24**, 671, 2006.
7. Levesque, J.P., Winkler, I.G., Hendy, J., Williams, B., Helwani, F., Barbier, V., Nowlan, B., and Nilsson, S.K. Hematopoietic progenitor cell mobilization results in hypoxia with increased hypoxia-inducible transcription factor-1 alpha and vascular endothelial growth factor A in bone marrow. *Stem Cells* **25**, 1954, 2007.
8. Kiprilov, E.N., Awan, A., Desprat, R., Velho, M., Clement, C.A., Byskov, A.G., Andersen, C.Y., Satir, P., Bouhassira, E.E., Christensen, S.T., and Hirsch, R.E. Human embryonic stem cells in culture possess primary cilia with hedgehog signaling machinery. *J Cell Biol* **180**, 897, 2008.
9. Denk, W., Strickler, J.H., and Webb, W.W. 2-Photon laser scanning fluorescence microscopy. *Science* **248**, 73, 1990.
10. So, P.T.C., Dong, C.Y., Masters, B.R., and Berland, K.M. Two-photon excitation fluorescence microscopy. *Ann Rev Biomed Eng* **2**, 399, 2000.
11. Zoumi, A., Yeh, A., and Tromberg, B.J. Imaging cells and extracellular matrix *in vivo* by using second-harmonic generation and two-photon excited fluorescence. *Proc Natl Acad Sci U S A* **99**, 11014, 2002.
12. Zipfel, W.R., Williams, R.M., Christie, R., Nikitin, A.Y., Hyman, B.T., and Webb, W.W. Live tissue intrinsic emission microscopy using multiphoton-excited native fluorescence and second harmonic generation. *Proc Natl Acad Sci U S A* **100**, 7075, 2003.
13. Plotnikov, S.V., Millard, A.C., Campagnola, P.J., and Mohler, W.A. Characterization of the myosin-based source for second-harmonic generation from Muscle sarcomeres. *Biophys J* **90**, 693, 2006.
14. Campagnola, P.J., and Loew, L.M. Second-harmonic imaging microscopy for visualizing biomolecular arrays in cells, tissues and organisms. *Nat Biotechnol* **21**, 1356, 2003.
15. Squirrell, J.M., Wokosin, D.L., White, J.G., and Bavister, B.D. Long-term two-photon fluorescence imaging of mammalian embryos without compromising viability. *Nat Biotechnol* **17**, 763, 1999.
16. Lee, H.S., Huang, G.T., Chiang, H.S., Chiou, L.L., Chen, M.H., Hsieh, C.H., and Jiang, C.C. Multipotential mesenchymal stem cells from femoral bone marrow near the site of osteonecrosis. *Stem Cells* **21**, 190, 2003.
17. Griffon, D.J., Sedighi, M.R., Schaeffer, D.V., Eurell, J.A., and Johnson, A.L. Chitosan scaffolds: interconnective pore size and cartilage engineering. *Acta Biomater* **2**, 313, 2006.
18. Lee, H.S., Teng, S.W., Chen, H.C., Lo, W., Sun, Y., Lin, T.Y., Chiou, L.L., Jiang, C.C., and Dong, C.Y. Imaging human bone marrow stem cell morphogenesis in polyglycolic acid scaffold by multiphoton microscopy. *Tissue Eng* **12**, 2835, 2006.
19. Nettles, D.L., Elder, S.H., and Gilbert, J.A. Potential use of chitosan as a cell scaffold material for cartilage tissue engineering. *Tissue Eng* **8**, 1009, 2002.

20. Chen, W.L., Li, T.H., Su, P.J., Chou, C.K., Fwu, P.T., Lin, S.J., Kim, D., So, P.T.C., and Dong, C.Y. Second harmonic generation chi tensor microscopy for tissue imaging. *Appl Phys Lett* **94**, 183, 2009.

Address correspondence to:

Hsuan-Shu Lee, M.D.

*Department of Internal Medicine
National Taiwan University Hospital*

*No. 7, Chung-Shan South Road
Taipei 100*

Taiwan

E-mail: benlee@ntu.edu.tw

*Chen-Yuan Dong, Ph.D.
Department of Physics
National Taiwan University
Taipei 106
Taiwan*

E-mail: cydong@phys.ntu.edu.tw

Received: September 4, 2009

Accepted: November 12, 2009

Online Publication Date: January 11, 2010

This article has been cited by:

1. Roman Dittmar, Esther Potier, Marc van Zandvoort, Keita Ito. 2012. Assessment of Cell Viability in Three-Dimensional Scaffolds Using Cellular Auto-Fluorescence. *Tissue Engineering Part C: Methods* **18**:3, 198-204. [[Abstract](#)] [[Full Text HTML](#)] [[Full Text PDF](#)] [[Full Text PDF with Links](#)]